REPORT DOCUMENTATION PAGE

Form Approved
OMB No. 0704-0188

1. AGENCY USE ONLY (Leave blank)	2. REPORT DATE	3. REPORT TYPE AND DATES COVERED
	September 23, 1996	Final Report 9/1/92 - 8/31/96

4. TITLE AND SUBTITLE

Mechanics of Localized Deformation of Solids Under Cyclic and Thermal Loadings

5. FUNDING NUMBERS

Grant No.
F49620-92-J-0370

6. AUTHOR(S)

T. H. Lin

7. PERFORMING ORGANIZATION NAME(S) AND ADDRESS(ES)

Univ of California, Los Angeles
405 Hilgard Avenue
Los Angeles, CA 90024-1406

AFOSR-TR-96
0536

9. SPONSORING/MONITORING AGENCY NAME(S) AND ADDRESS(ES)

AFOSR/~~NC~~
Building 410, Bolling AFB DC
20332-6448

NA

10. SPONSORING/MONITORING AGENCY REPORT NUMBER

92-J-0370

11. SUPPLEMENTARY NOTES

12a. DISTRIBUTION/AVAILABILITY STATEMENT

APPROVED FOR PUBLIC RELEASE; DISTRIBUTION IS UNLIMITED.

19961104 079

13. ABSTRACT *(Maximum 200 words)*

The student under the training program is first taught with the ground work of crystal physics and the transformation of axes in second-rank tensors. Then he has participated in different topics in the parent research grant (F49620-92-J-0171), "Mechanics of Localized Deformation of Solids under Cyclic Mechanical and Thermal Loadings".

He has contributed more in the following two areas: (1) Effect of single crystal elastic anisotropy on the fatigue band deformation in polycrystals. The application of Eshelby's Equivalent Inclusion Method to transform an inhomogeneous solid into a homogeneous one in shown and a numerical example is given. (2) The analysis of the growth of extrusions in a single crystal is shown. The boundary tractions of a most favorably oriented crystal at the free surface of a polycrystal are removed to simulate a single crystal. The calculated extrusions are compared with those observed subgrain boundary movements.

14. SUBJECT TERMS			15. NUMBER OF PAGES 22
			16. PRICE CODE
17. SECURITY CLASSIFICATION OF REPORT	18. SECURITY CLASSIFICATION OF THIS PAGE	19. SECURITY CLASSIFICATION OF ABSTRACT	20. LIMITATION OF ABSTRACT
UNCLASSIFIED	UNCLASSIFIED	UNCLASSIFIED	

Final Technical Report

(AASERT) Mechanics of Localized Deformation of Solids under Cyclic and Thermal Loadings

Grant No. F49620-92-J-0370
September 1, 1992 - August 31, 1996
Program Manager: Dr. Brian Sanders

Department of Civil & Environmental Engineering
School of Engineering and Applied Sciences
University of California, Los Angeles

Principal Investigator:
T. H. Lin
Professor of Civil & Environmental Engineering

Student under this Program:
Kevin Wong

September 23, 1996

Outline

Final Technical Report

(AASERT) Mechanics of Localized Deformation of Solids under Cyclic and Thermal Loadings

Grant No. F49620-92-J-0370

9/01/92 - 8/31/96

Student under the Program: Kevin Wong +

Principal Investigator: T. H. Lin

Abstract

The student under the training program is first taught with the ground work of crystal physics and the transformation of axes in second-rank tensors. Then he has participated in different topics in the parent research grant (F49620-92-J-0171), "Mechanics of Localized Deformation of Solids under Cyclic Mechanical and Thermal Loadings".

He has contributed more in the following two areas: (1) Effect of single crystal elastic anisotropy on the fatigue band deformation in polycrystals. The application of Eshelby's Equivalent Inclusion Method to transform an inhomogeneous solid into a homogeneous one in shown and a numerical example is given. (2) The analysis of the growth of extrusions in a single crystal is shown. The boundary tractions of a most favorably oriented crystal at the free surface of a polycrystal are removed to simulate a single crystal. The calculated extrusions are compared with those observed subgrain boundary movements.

+ He has been awarded Ph.D. degree in Civil Engineering and is currently a postdoctrate in the Civil Engineering Department at UCLA.

I. Introduction

Single crystals under loading slide along certain directions on certain planes. This slip depends on the resolved shear stress in the slip system and is independent of the normal pressure on the sliding plane. This crystal characteristic is known as the Schmid's law. This Schmid's law also holds under cyclic loading (Parker, 1961). In a face-centered cubic (fcc) material, there are four slip planes, on each of which there are three slip directions, giving a total of twelve slip systems. A micromechanic theory of fatigue crack initiation has been developed to model the gating mechanism of fatigue band in polycrystals (Lin and Ito, 1969; Lin 1992). A fatigue band is composed of three thin slices P, Q, and R in a most favorably oriented surface crystal (Figure 1) was considered. Lin (1992) has shown that cyclic tension and compression loading causes alternate monotonic buildup of plastic shear strains in both P and Q to form a persistent slip band (PSB). This, in turn, causes the growth of extrusions and intrusions (Forsyth and Stubbington, 1955) at the free surface of the polycrystal.

These PSB's are preferred sites of fatigue crack initiation. Hence, the depth of intrusion and the height of extrusion are taken as a measure of the fatigue damage. The thickness of the slices P, Q, and R is much smaller than their length (along x_3-axis). The plastic strain caused by slip in the central part of the band is close to being constant along the length, so the central portion of the band is considered to be under plane deformation.

All metals have initial defects, and have initial stresses. These initial stresses play an important role in fatigue crack initiation. Lin and Ito (1969) first point out;that the initial stress field favorable to extrusions and intrusions can be caused by a row of dislocation dipoles. Later, these dislocation dipoles have been observed in the ladder structure in persistent slip bands (Antonopoulos, 1976; Mughrabi, 1981). These dipoles induce initial resolved shear stresses at the interface between the PSB and the matrix.

Extrusion causes elongation and a tensile stress in R. This stress combined with applied cyclic stress can activate a second slip system to slide. This slip in the secondary slip system enhances the extent of extrusion (Lin *et al.*, 1989). Interchanging the signs of the initial stresses in P and Q initiates an intrusion instead of an extrusion. This theory of fatigue crack initiation has overwhelming metallurgical evidences (Lin, 1977).

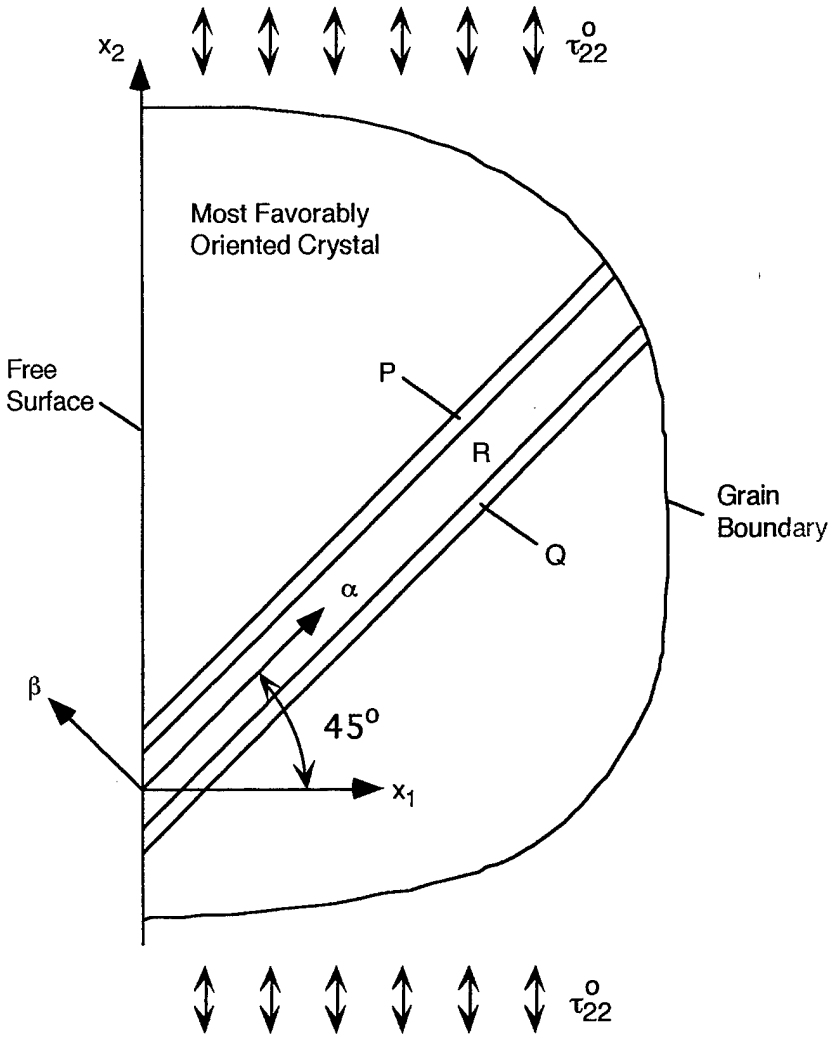

Figure 1
Fatigue band in the most favorably oriented surface crystal.

II. Elastic Anisotropy of Crystal in Polycrystal Fatigue Band Formation

The above model mainly concerned with the fatigue crack initiation of aluminum and its alloys. The elastic anisotropy of their individual crystals is insignificant and accordingly neglected. Hence, this surface crystal is assumed to be embedded in an elastically isotropic and homogeneous semi-infinite medium. Thus this problem is reduced to an anisotropic inclusion in an elastic isotropic semi-infinite solid. This heterogeneous solid is then transformed into a homogeneous one using Eshelby's Equivalent Inclusion Method by introducing an extra set of eigenstrain

(Eshelby, 1957; Mura, 1982). Then the calculation of stress and strain fields can be carried out in the same way as for a single phase solid.

A method of inelastic analysis of elastic isotropic homogeneous solids has been developed by Lin and Ito (1966) and Lin (1971). The residual stress $\tau_{ij}^r(\mathbf{x})$ at a point $\mathbf{x}$ in an infinite elastic isotropic medium caused by a unit plastic strain $e_{kl}^p(\mathbf{x}')$ in an elemental volume $\Delta v'$ at $\mathbf{x}'$ is expressed as (Lin, 1971)

$$\tau_{ij}^r(\mathbf{x}) = G_{ijkl}(\mathbf{x},\mathbf{x}')e_{kl}^p(\mathbf{x}')\,\Delta v' \tag{1}$$

where $\Delta v'$ is an elemental volume and $G_{ijkl}(\mathbf{x},\mathbf{x}')$ is the influence coefficient of the stress $\tau_{ij}^r(\mathbf{x})$ at $\mathbf{x}$ caused by unit plastic strain $e_{kl}^p(\mathbf{x}')$ in $\mathbf{x}'$. In the following, $\Delta v'$ is omitted to simplify writing. Consider first a homogeneous isotropic solid subject to a uniform loading; i.e., the surface traction S_i along x_i-axis per unit area with an exterior normal ν equals $\tau_{ij}^o\,\nu_j$. The stress is uniform and equal to τ_{ij}^o with a corresponding strain e_{ij}^o. If this body has subdomain Ω in the region D-Ω, as shown in Figure 2, with elastic moduli C_{ijkl}^* different from those of D-Ω denoted by C_{ijkl}, this inclusion would give a disturbance strain $\bar{e}_{ij}$ and disturbance stress $\bar{\tau}_{ij}$. Now the stress in Ω would be $C_{ijkl}^*(e_{ij}^o + \bar{e}_{ij})$ and that in D-Ω would be $C_{ijkl}(e_{ij}^o + \bar{e}_{ij})$.

Eshelby (1957, 1961) ingeniously pointed out that this disturbance stress $\bar{\tau}_{ij}$ can be simulated by an inelastic strain, referred to as an eigenstrain e_{ij}^* (Mura, 1982) to differentiate it from the inelastic strain which commonly represent the plastic and creep strain. If we let

$$\tau_{ij}^r = C_{ijkl}(e_{kl}^o + \bar{e}_{kl} - e_{kl}^*) = C_{ijkl}^*(e_{kl}^o + \bar{e}_{kl}) \quad \text{in } \Omega \tag{2}$$

we can replace the subdomain with C_{ijkl}^* by one with C_{ijkl}. After this imaginary replacement, we have a homogeneous solid with elastic moduli C_{ijkl}. e_{ij}^* has the same effect as e_{ij}^p in causing residual stress. We have from Eq. (1)

$$C_{ijkl}\left[\bar{e}_{kl}(\mathbf{x}) - e_{kl}^*(\mathbf{x})\right] = G_{ijkl}(\mathbf{x},\mathbf{x}')e_{kl}^*(\mathbf{x}') \tag{3}$$

Let S_{ijkl} be the elastic compliance of the region D-Ω. From Eqs. (2) and (3),

$$\bar{e}_{kl}(\mathbf{x}) = S_{ijkl}\,G_{ijkl}(\mathbf{x},\mathbf{x}')e_{kl}^*(\mathbf{x}') + e_{kl}^*(\mathbf{x}') \tag{4}$$

$$C_{ijkl}^* e_{kl}^o + C_{ijkl}^*\left[S_{klmn}G_{mnrs}(\mathbf{x},\mathbf{x}')e_{rs}^*(\mathbf{x}') + e_{kl}^*(\mathbf{x}')\right] = \tau_{ij}^o + G_{ijkl}(\mathbf{x},\mathbf{x}')e_{kl}^*(\mathbf{x}') \tag{5}$$

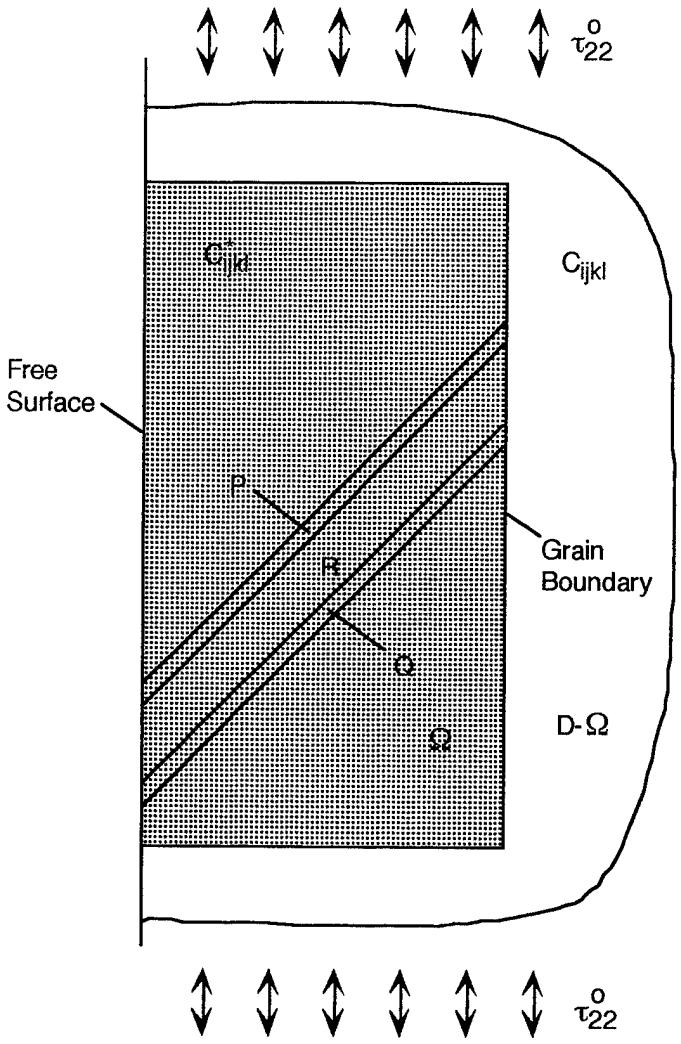

Figure 2
Anisotropic surface crystal embedded in an isotropic semi-infinite medium.

This gives the solution of $e^*_{kl}(\mathbf{x}')$. If we have plastic strain e^p_{ij}, Eqs. (2) and (4) become

$$C^*_{ijkl}(e^o_{kl} - e^p_{kl} + \bar{e}_{kl}) = C_{ijkl}(e^o_{kl} - e^p_{kl} + \bar{e}_{kl} - e^*_{kl}) \tag{6}$$

$$\bar{e}_{kl}(\mathbf{x}) = S_{ijkl}\, G_{ijkl}(\mathbf{x}, \mathbf{x}')\left[e^p_{kl}(\mathbf{x}') + e^*_{kl}(\mathbf{x}')\right] + e^p_{kl}(\mathbf{x}') + e^*_{kl}(\mathbf{x}') \tag{7}$$

$$\begin{aligned} C^*_{ijkl}\, e^o_{kl} + C^*_{ijkl}\left\{S_{klmn}\, G_{mnrs}(\mathbf{x},\mathbf{x}')\left[e^p_{rs}(\mathbf{x}') + e^*_{rs}(\mathbf{x}')\right] + e^*_{kl}(\mathbf{x}')\right\} \\ = \tau^o_{ij} + G_{ijkl}(\mathbf{x},\mathbf{x}')\left[e^p_{kl}(\mathbf{x}') + e^*_{kl}(\mathbf{x}')\right] \end{aligned} \tag{8}$$

With $e^p_{ij}(\mathbf{x}')$ known, Eq. (8) gives the solution of $e^*_{ij}(\mathbf{x}')$.

This method was applied to find the plastic strain distribution in a fatigue band in the most favorably oriented crystal located at a free surface of the polycrystal. The surface crystal was considered to have anisotropic elastic constants C^*_{ijkl} and the remaining part of the polycrystal was assumed to be elastically isotropic, as shown in Figure 2. In the numerical calculation, the anisotropic surface crystal, including the thin slices P, Q, and R was divided into a number of elements. Plastic deformation is highly concentrated in the fatigue band. There is no plastic strain outside P, Q, and R. By using the method described above, the eigenstrain e^*_{ij}, which is used to transform the heterogeneous body into a homogeneous one, is composed of two parts, one from the applied load and the other from the plastic strain. The contribution of these parts lead to the change of Schmidt factors and stress influence coefficients, and hence the slip distributions in the bands.

In the following numerical calculation, these closely located thin slices P, Q, and R in the crystal are considered to have a small positive initial resolved shear stress in P and a negative one in Q. The anisotropic elastic constants of Ni_3Al intermetallic compound, experimentally obtained by Yang (1985), are used. The isotropic elastic constants of the surrounding metal composed of crystals of random orientation are obtained by a conventional approximate average methods such as Voigt or Reuss methods. Assuming the strain-hardening in P and Q to be zero and using the numerical method developed by Lin *et al.* (1989), we have obtained some preliminary plastic strain distributions in the fatigue band under cyclic tension and compression at 10 and 20 cycles as shown in Figure 3. This effect of elastic anisotropy will be further studied for the cases of multiple fatigue band in the most favorably oriented crystal and on the propagation of the fatigue band across the grain boundary. The heterogeneous inclusion causes a varying stress field in the body under uniform loadings τ_{22}. The Schmidt factor in the bands is 0.5 if the solid is homogeneous and isotropic. With the anisotropic inclusion C^*_{ijkl}, the Schimdt factor varies along the bands. The part of the band with this Schmidt factor greater than 0.5 will slide and start to form a fatigue band. This will cause different distributions of plastic strain in P and Q and affect considerably the growth of fatigue band of the material.

The microstress of the fatigue band in the surface crystal depends not only on the anisotropic elastic constants of the crystal, but also on these anisotropic constants of all the crystals. The previous study considers only the elastic anisotropy of the surface crystal. Further study considers also the elastic anisotropy of the surrounding crystals. The details of the analysis and the results are given in the paper "Elastic Anisotropy Effect of Crystals on Polycrystal Fatigue Crack Initiation", published in the Journal of Engineering Materials and Technology, ASME, Vol. 117, No. 4, pp. 470-477. A copy of the paper is given in the appendix.

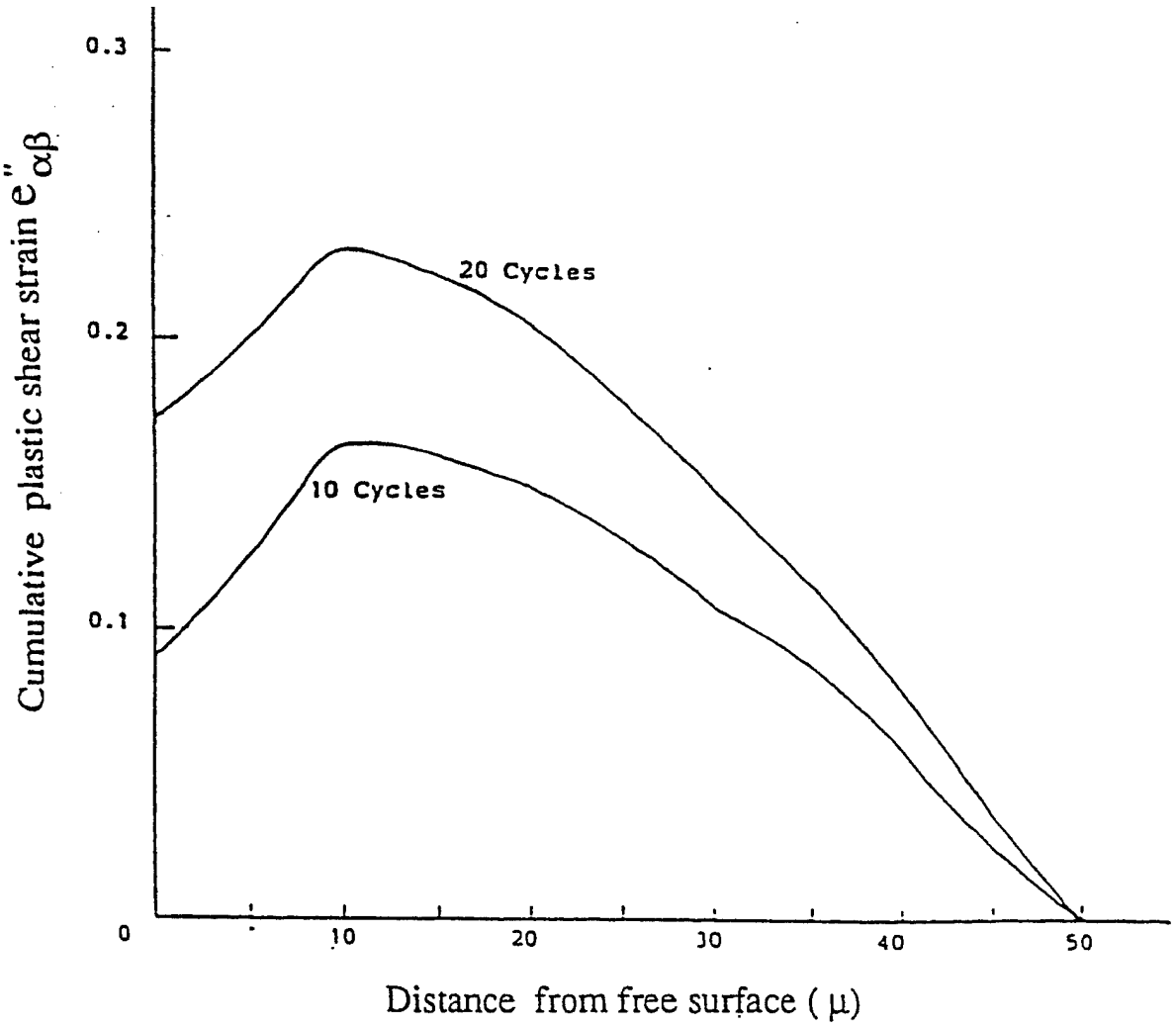

Figure 3
Plastic shear strain distribution along band considering band anisotropy in the surface crystal.

III. Fatigue Bands in Single Crystal

Single crystals are often used in jet engines. Extrusions and intrusions in PSBs have been observed in these single crystals under high-cycle fatigue (HCF) loadings. These PSBs are the preferred sites of fatigue crack initiation. Hence this study is of both scientific interest and engineering needs.

The growth of extrusion and intrusion in polycrystal of elastic isotropy has been studied by Lin and his associates (Lin *et al.*, 1989; Lin, 1992). To analyze this growth in a polycrystal, the fatigue bands are assumed to occur in a most favorably oriented crystal embedded at a free surface of the metal. The analysis is reduced to a plane strain solution of a semi-infinite elastically

isotropic solid. The cross-section of the single crystal is assumed to be rectangular (Figure 4) with "b" considerably larger than "a". The deformation of the center portion will be close to plane strain. The fatigue band in this portion is considered to represent that of the single crystal. Using the solution of fatigue bands in polycrystal (Lin, 1992), we obtain the stress field of this surface crystal with boundary tractions as shown in Figure 5(a). To find the stress field due to this slid grid in the single crystal, these boundary tractions are to be relieved by a set of equal and opposite tractions using finite element method (FEM), as shown in Figure 5(b). The sum of the stresses given by Figures 5(a) and 5(b) gives the residual stress field due to the slid grid, as shown in Figure 5(c).

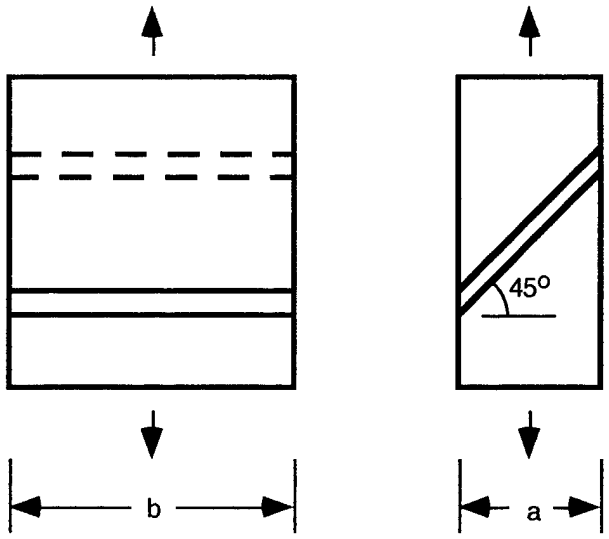

Figure 4
Single crystal under cyclic tension and compression loadings.

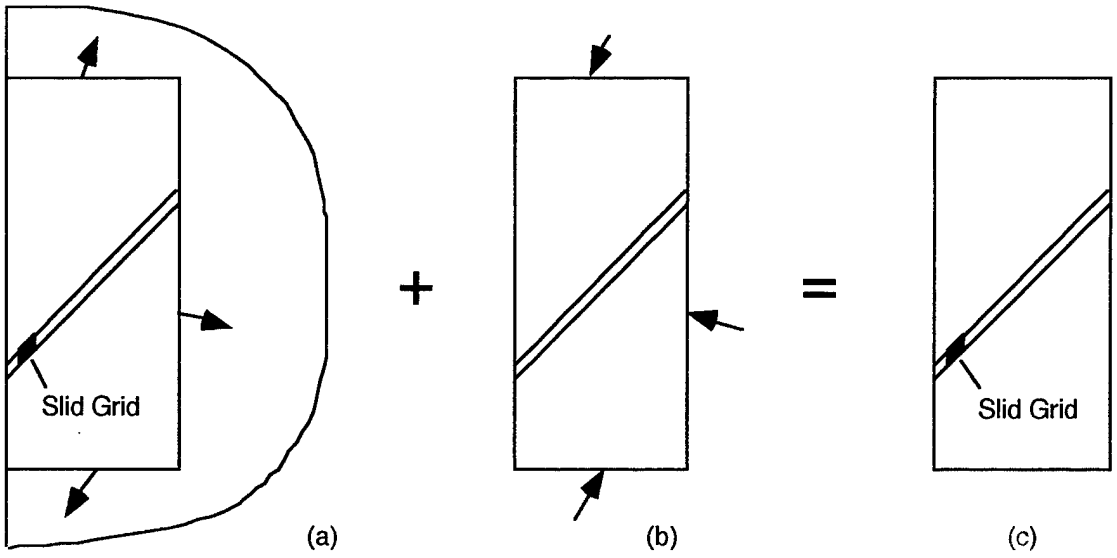

Figure 5
Superposition of semi-infinite plane strain solution and finite element solution.

The localization of the surface traction (Figure 5(b)) depends on the distance of the slid grid from the boundary. The amount of numerical work and the difficulty of the FEM to achieve a given accuracy depends on the distance. Hence, for a slid grid in the left half of the crystal, as shown in Figure 5(a), the free surface of the semi-infinite solid is taken on the left. Similarly, for a slid grid in the right half, the free surface is taken to be on the right. By this way, the boundary traction would be much less localized. This would facilitate greatly the FEM calculations.

In 1980, Mecke and Blochwitz performed an experiment using nickel single crystal to study the behavior of PSBs under cyclic loadings. This experiment was conducted at room temperature and at a constant plastic strain amplitude of $e_{ap} = 1.3\text{x}10^{-3}$. The result is shown in Figure 6 after many cycles of loadings. This figure shows that both the PSBs and the subgrain boundaries (SGB), 1 to 2 μm each in width, have penetrated across the whole crystal and extruded from both sides.

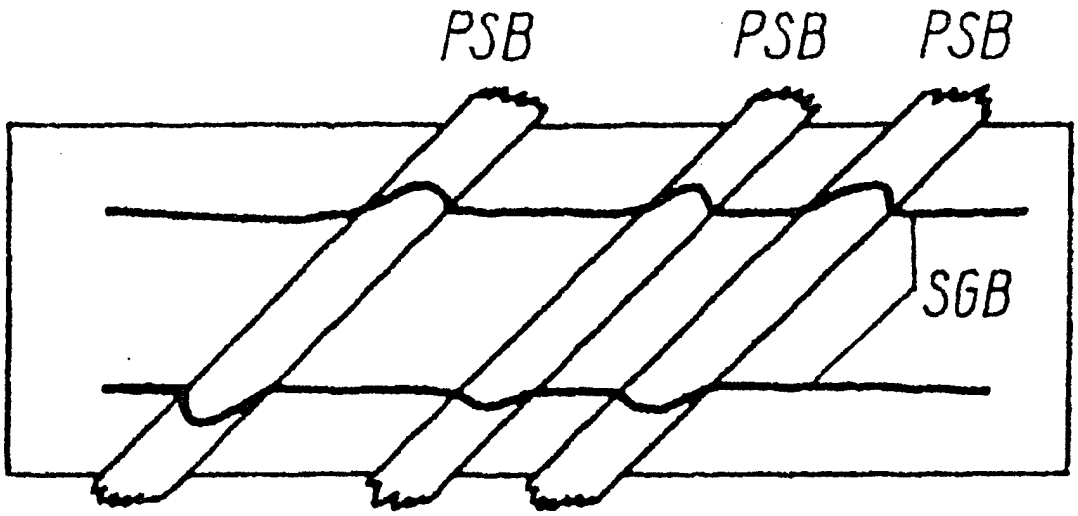

Figure 6
Extrusions observed in single crystal.

Using the numerical method developed as described, we consider a seven band face-centered cubic single crystal loaded in cyclic tension and compression. This model is shown in Figure 7. The most favorably slip system, called the primary slip system, makes an angle of 45° with the specimen axis. As in the previous models (Figure 1), each fatigue band is composed of three thin slices. These slices in the left half are denoted by P, Q, and R, and those in the right half are denoted by P', Q', and R'. As R and R' extrudes, a second slip system may be activated. This crystal is assumed to be elastically isotropic. The shear modulus μ is taken to be 50 GPa and Poisson's ratio is taken to be 0.3. The critical shear strength σ^c is assumed to be 200 MPa and the applied stress σ_{22} is 400 MPa.

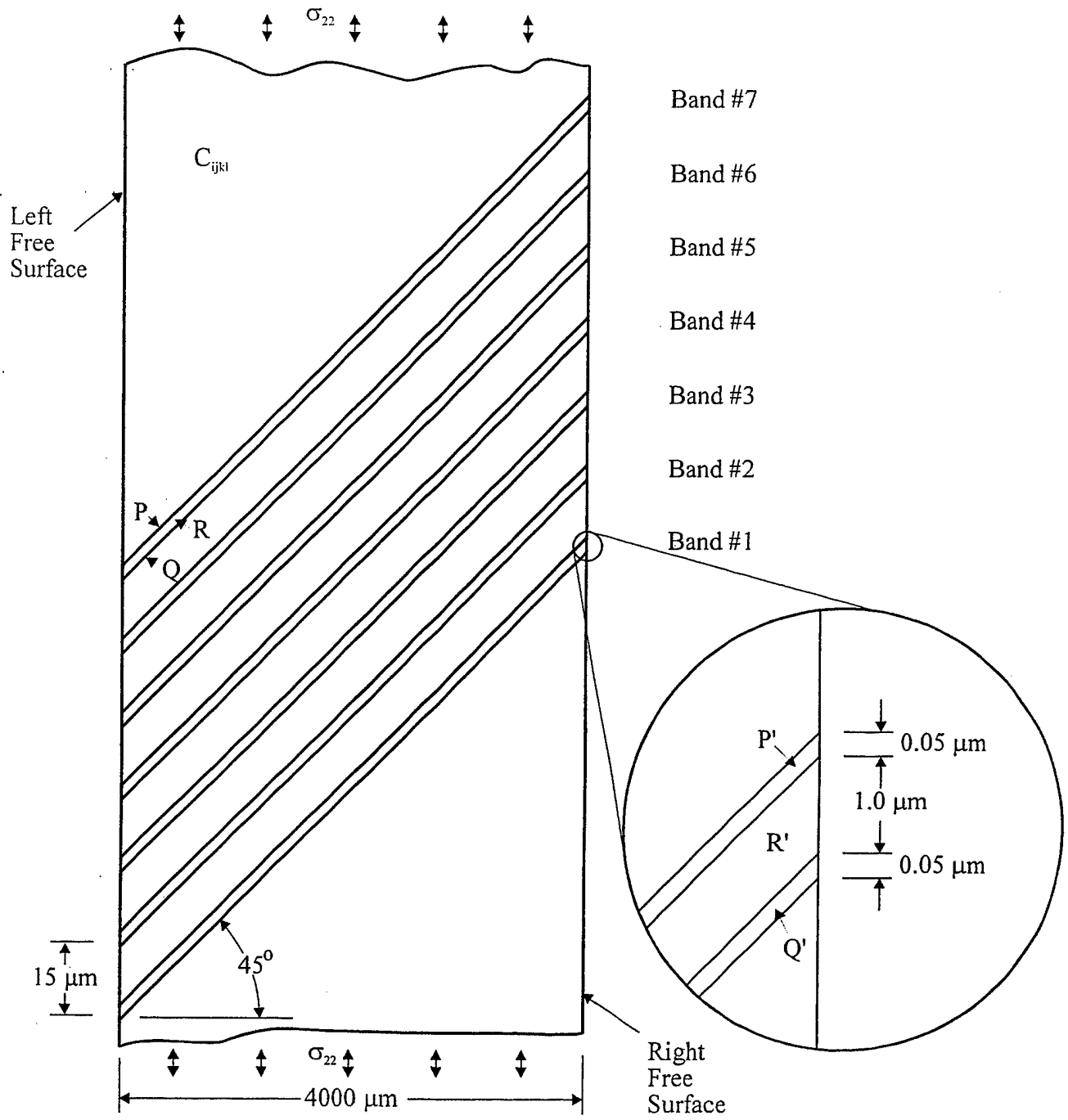

Figure 7
Isotropic seven band model of the single crystal.

To see the effect of the location of initial tensile strain in R on the extrusion growth, the grid with this initial strain was taken to be in the left, then at the center, and finally at the right portion of a single fatigue band. The calculated plastic strain variations with the number of loading

cycles are shown in Figure 8. All three locations show positive shear strain in P and a negative one in Q, showing the occurrence of extrusions.

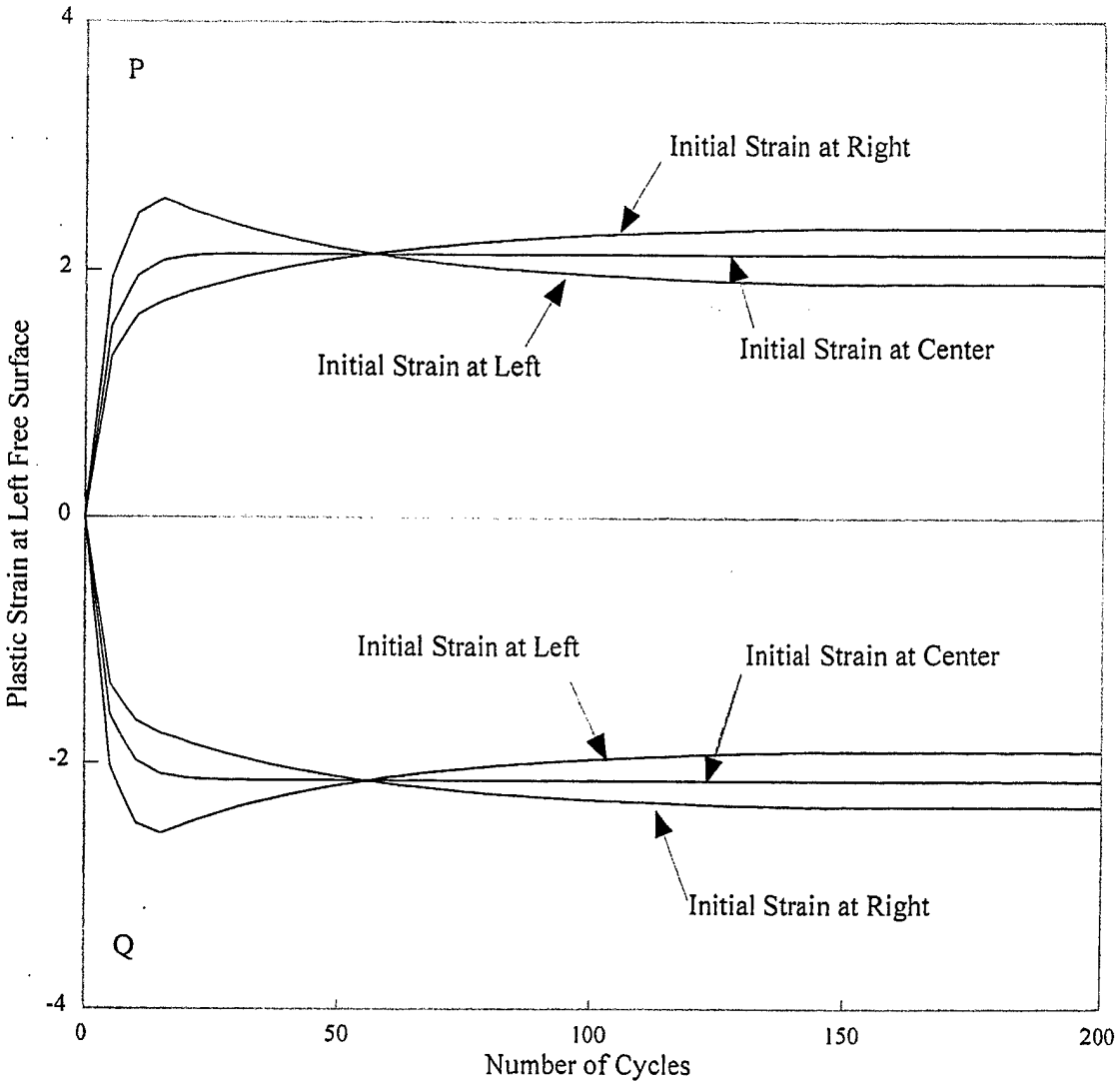

Figure 8
Plastic strain distribution at left free surface.

Then the initial tensile stress at the center and the applied cyclic loadings are increased until the plastic strain occur in both the primary and secondary slip systems. These primary and secondary plastic strains variations along the band at different loading cycles are shown in Figure 9 and 10, respectively.

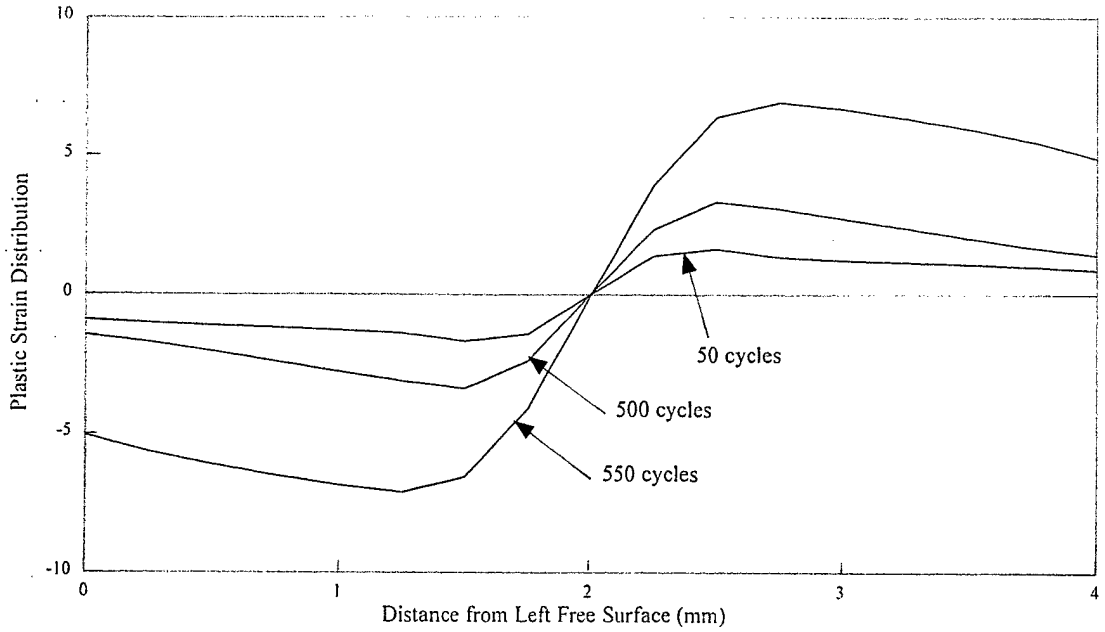

Figure 9
Plastic strain in primary slip system of Q.

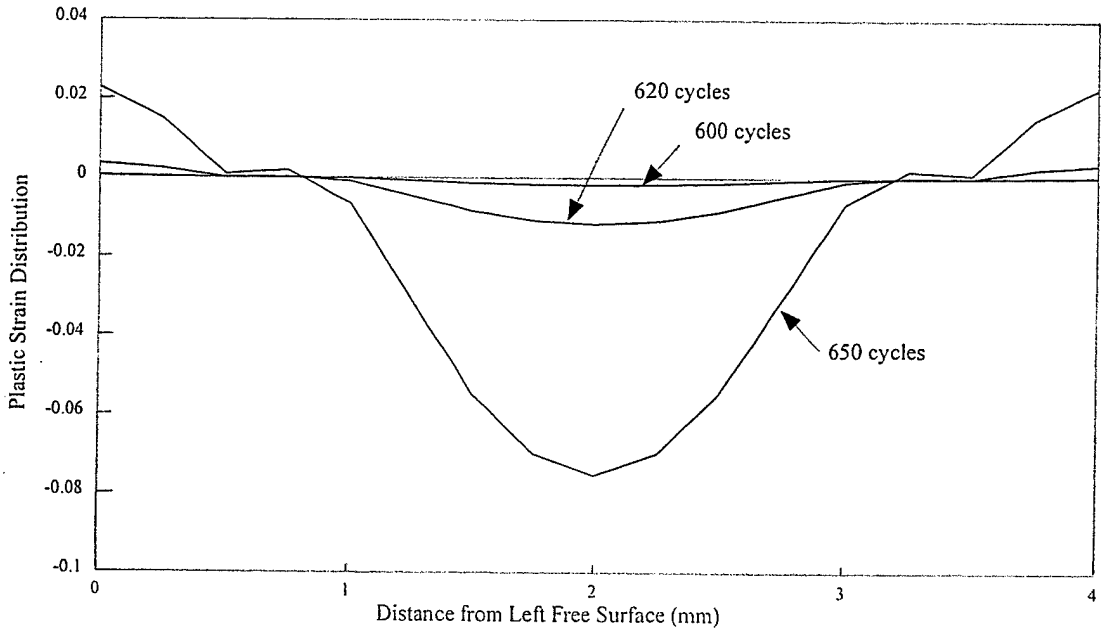

Figure 10
Plastic strain in secondary slip system of R.

These gives some preliminary results of HCF bands in single crystal.

IV. References

Antonopoulos J.G., Brown L.M., and Winter A.T. (1967), "Vacancy Dipoles in Fatigued Copper", *Phil. Mag.*, Vol. 34, p. 549.

Eshelby J.D. (1957), "The Determination of the Elastic Field of an Ellipsoidal Inclusion and Related Problems", *Proc. Roy. Soc. (A)*, Vol. 241, pp. 376-396.

Eshelby J.D. (1961), "Elastic Inclusions and Inhomogeneities", *Progress in Solid Mechanics*, Vol. II, edited by I.N. Sneddon and R. Hill, North Holland Publishing Co., pp. 89-139.

Forsyth P.J.E. and Stubbington C.A. (1955), "The Slip Band Extrusion Effect Observed in Some Aluminum Alloys Subjected to Cyclic Stresses", *J. Inst. Metals*, Vol. 83, p. 395.

Lin T.H. and Ito Y.M. (1966), "Theoretical Plastic Deformation of Polycrystal and Comparisons with von Mises and Tresca's Plasticity Theories", *Int. J. Eng. Sci.*, Vol. 4 , pp. 543-561.

Lin T.H. and Ito Y.M. (1969), "Fatigue Crack Nucleation in Metals", *Proc. U.S. Natl. Acad. Sci.*, Vol. 64, pp. 631-635.

Lin T.H. (1971), "Physical Theory of Plasticity", *Advances in Applied Mechanics*, edited by C.S. Yih, Academic Press, Vol. 11, pp. 255-307.

Lin T.H. (1977), "Micromechanics of Deformation of Slip Bands under Monotonic and Cyclic Loading", Reviews on the Deformation Behavior of Materials, edited by P. Feltham, Freund Publishing House, Tel-Aviv, Israel, pp. 263-316.

Lin T.H., Lin S.R., and Wu X.Q. (1989), "Micromechanics of an Extrusion in High-Cycle Fatigue", *Phil. Mag. A*, Vol. 59, pp. 1263-1276.

Lin T.H. (1992), "Micromechanics of Crack Initiation in High-Cycle Fatigue", *Advances in Applied Mechanics*, Vol. 29, pp. 1-68.

Mecke K. and Blochwitz C. (1980), "Internal Displacements of Persistent Slip Bands in Cyclically Deformed Nickel Single Crystals", *Phys. Stat. Sol. (A)*, Vol. 64, K5.

Mughrabi H. (1981), "Cyclic Plasticity of Matrix and Persistent Slip Bands in Fatigued Metals", *Continuum Model for Discrete Systems 4*, edited by O. Brulin and R.K.T. Hsieh, North Holland, pp. 241-257.

Mura T. (1982), *Micromechanics of Defects in Solids*, Martinus Nijhoff Publishers, pp. 1-6, 151-159.

Parker E.R. (1961), "Theory of Fatigue", Mechanical Behavior of Materials at Elevated Temperatures, edited by J.E. Dorn, McGraw-Hill, New York, pp. 129-148.

Yang S.W. (1985), "Elastic Constants of a Monocrystalline Nickel-Base Superalloy", *Meta. Trans. A*, Vol. 16A, pp. 661-665.

V. Appendix: Reprints

Teng N.J. and Lin T.H., "Elastic Anisotropy Effect of Crystals on Polycrystal Fatigue Crack Initiation", *J. Eng. Materials and Technology, Trans. ASME*, pp. 470-477, 1995.

Elastic Anisotropy Effect of Crystals on Polycrystal Fatigue Crack Initiation

N. J. Teng

T. H. Lin

Department of Civil and Environmental Engineering,
University of California, Los Angeles,
Los Angeles, CA 90024

Fatigue bands have been observed in both monocrystalline and polycrystalline metals. Extrusions and intrusions at the free surface of fatigued specimens are favorable sites for fatigue crack nucleation. Previous studies (Lin and Ito, 1969; Lin, 1992) mainly concerned the fatigue crack initiation in aluminum and its alloys. The elastic anisotropy of individual crystals of these metals is insignificant and was accordingly neglected. However, the anisotropy of the elastic constants of some other metallic crystals, such as titanium and some intermetallic compounds, is not negligible. In this paper, the effect of crystal anisotropy is considered by using Eshelby's equivalent inclusion method. The polycrystal analyzed is Ni_3Al intermetallic compound. The plastic shear strain distributions and the cumulative surface plastic strain in the fatigue band versus the number of loading cycles were calculated, and the effect of crystal anisotropy on the growth of the extrusions was examined.

1 Introduction

The process of fatigue failure in ductile metals is divided into the following three stages: (1) the crack initiation, (2) the growth and coalescence of microcracks to form some macrocracks, and (3) the propagation of dominant cracks leading to the final catastrophic failure. In high-cycle fatigue, fatigue crack initiation predominates fatigue life. Fatigue bands are the favorable sites for the nucleation of fatigue microcracks.

Fatigue bands consist of highly localized plastic strains and have been observed in both single crystals and polycrystals. Plastic strains are mainly due to the movement of dislocations. Under the cyclic loading, the localized plastic deformation increases with the number of loading cycles and causes extrusions and intrusions at the free surface of metals. The height of extrusions or the depth of intrusions is here taken as a measure of fatigue damage.

A theory of micromechanics of fatigue crack initiation has been proposed to model the gating mechanism of fatigue bands in polycrystals (Lin and Ito, 1969; Lin, 1992). A fatigue band composed of three thin slices P, Q, and R in a most favorably oriented surface crystal was considered. Under cyclic tension and compression loading, the alternate monotonic build-up of plastic shear strains in both P and Q causes the growth of extrusions or intrusions at the free surface of polycrystals. Since this model is concerned mainly with the fatigue crack initiation of aluminum and its alloys, the elastic anisotropy of their individual crystals is insignificant and accordingly neglected. Hence the surface crystal is assumed to be embedded in an elastically isotropic and homogeneous semi-infinite medium. For some other polycrystalline metals, such as titanium and some intermetalic superalloys, however, the elastic anisotropy of crystals is not negligible. For such polycrystals, the local microstress field in a crystal depends not only on the applied stresses but also on the orientations of its surrounding crystals. Hence the elastic anisotropy of crystals will affect the fatigue crack initiation in these metals.

In this paper, the elastic anisotropy of individual grains in a polycrystal is considered. A fatigue band is assumed to occur in the most favorably oriented surface crystal. This crystal is surrounded by the crystals of various given orientations. The crystals outside the surrounding crystals are randomly oriented and assumed to be isotropic and homogeneous. Hence this surface crystal and the surrounding crystals of given orientations are considered to be embedded in a semi-infinite isotropic and homogeneous elastic medium. Thus it becomes an inclusion problem. This heterogeneous solid is transformed into a homogeneous one by using Eshelby's equivalent inclusion method (Eshelby, 1957, 1961; Mura, 1982). In this method, an extra set of eigenstrains is introduced. These eigenstrains can be explicitly expressed in terms of the applied stresses and plastic strains. After this transformation, the procedures for this micromechanical analysis are the same as those given by Lin (1992) for elastically isotropic polycrystals. In the following numerical calculation, the anisotropic elastic constants of Ni_3Al monocrystalline intermetallic compound (Yang, 1985) were used. The isotropic elastic constants of the surrounding metal were taken from the experimental data (Stoloff, 1989). The plastic strain distributions and the cumulative surface plastic strains in the fatigue band versus the number of loading cycles were calculated, and the effect of elastic anisotropy on the formation of extrusions and intrusions was examined.

2 Gating Mechanism Provided by Microstress Field

Single crystal tests show that slip occurs on certain crystallographic planes along certain directions. This slip depends on the resolved shear stress in the slip system and is independent of the normal stress on the sliding plane. The dependence of slip on the resolved shear stress is known as the Schmid law. It has been shown that the Schmid law also holds when crystalline solids are subjected to cyclic loading (Parker, 1961). For a face-centered cubic crystal (FCC), there are four slip planes, on each of which, there are three slip systems. These twelve slip systems are shown in Fig. 1.

All metals have initial defects, hence, have initial stresses. These initial stresses play an important role in fatigue crack initiation. Lin and Ito (1969) first point out that the initial stress field favorable to extrusions and intrusions can be caused by a row of dislocation dipoles. Later, these dislocation dipoles have been observed in the ladder structure in a persistent slip band (PSB) (Antonopoulos, 1976; Mughrabi, 1982). These dipoles induce initial resolved shear stresses at the interface between the PSB and the matrix.

Based on experimental observations, a micromechanic theory of fatigue crack initiation was proposed by Lin and Ito (1969).

Contributed by the Materials Division for Publication in the JOURNAL OF ENGINEERING MATERIALS AND TECHNOLOGY. Manuscript received by the Materials Division June 3, 1995. Associate Technical Editor: G. J. Weng.

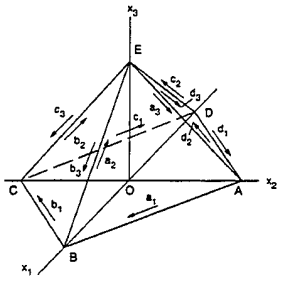

Slip Systems and Their Directions

Slip System	Slip Plane	Slip Directon
a_1		[1 $\bar{1}$ 0]
a_2	(1 1 1)	[$\bar{1}$ 0 1]
a_3		[0 1 $\bar{1}$]
b_1		[$\bar{1}$ $\bar{1}$ 0]
b_2	(1 $\bar{1}$ 1)	[0 1 1]
b_3		[1 0 $\bar{1}$]
c_1		[$\bar{1}$ 1 0]
c_2	($\bar{1}$ $\bar{1}$ 1)	[1 0 1]
c_3		[0 $\bar{1}$ $\bar{1}$]
d_1		[1 1 0]
d_2	($\bar{1}$ 1 1)	[0 $\bar{1}$ 1]
d_3		[$\bar{1}$ 0 $\bar{1}$]

Fig. 1 Crystallographic slip planes and directions of FCC crystals

In this model, a most-favorably oriented surface crystal containing a fatigue band composed of three thin slices P, Q, and R in a semi-infinite polycrystal shown in Fig. 2 is considered. The slip plane and slip direction of the primary slip system $\alpha\beta$ form an angle of 45 deg with the loading axis. Lin and Lin (1983) have calculated a uniform initial resolved shear stress field τ^I, positive in P and negative in Q, caused by a distribution of plastic strains. This initial stress field satisfies the conditions of both compatibility and equilibrium. During the cyclic loading, plastic strains occur in P, Q and R and cause a residual stress field. The total resolved shear stress τ in a slip system is the sum of three stresses as

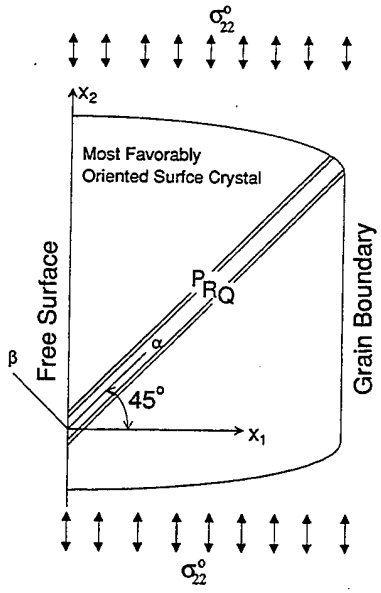

Fig. 2 Fatigue band in the most favorably oriented surface crystal

$$\tau = \tau^A + \tau^I + \tau^R$$

where τ^A is the resolved shear stress caused by the applied load and τ^R the residual resolved shear stress due to plastic strains.

A tensile loading σ^0_{22} on the polycrystal produces a positive τ^A in the entire surface crystal. Since τ^I in P is positive, the total resolved shear stress τ in P, which is $\tau^A + \tau^I$, reaches the critical shear stress τ^C first; and hence, according to Schmid law, P slides. The plastic shear strain caused by this slip in P produces a residual stress field τ^R, which has negative resolved shear stress in Q and makes Q to slide more readily in the reverse loading. The negative slip in Q induces in turn a positive residual resolved shear stress τ^R in P making P more readily to slide under the next tensile loading. This process is repeated during the cyclic loading for every cycle thus providing a natural gating mechanism for a monotonic buildup of local resolved plastic shear strain $e^p_{\alpha\beta}$ in both P and Q, pushing R out of the free surface and promoting an extrusion. The elongation of R may activate a secondary slip system to slide. The effect of slip in the secondary slip system enhances the extent of extrusion (Lin, et al., 1989). Interchanging the signs of the initial stresses in P and Q initiates an intrusion instead of an extrusion. This micromechanical theory on fatigue crack initiation has overwhelming metallurgical experimental evidences (Lin, 1977).

3 Calculation of Residual Stress Field

3.1 Residual Stress Field. The residual stress field due to a distribution of inelastic strains can be calculated by the analogy between inelastic strains and applied forces (Lin, 1969). It has been shown that the equivalent body force per unit volume along the x_i-axis due to inelastic strains ϵ''_{ij} is

$$\bar{F}_i = -C_{ijkl}\epsilon''_{kl,j} \tag{1}$$

where C_{ijkl} is the elastic modulus. The summation convention is used here and the subscript after a comma denotes the differentiation with respect to the coordinate variable. For isotropic elastic solids, the elastic constants are

$$C_{ijkl} = \lambda\delta_{ij}\delta_{kl} + \mu(\delta_{ik}\delta_{jl} + \delta_{il}\delta_{jk})$$

where λ and μ are Lame's constants and δ_{ij} is the Kronecker delta. The equivalent surface force per unit area along the x_i-axis has been shown as

$$\bar{S}_i = C_{ijkl}\epsilon''_{kl}\nu_j \tag{2}$$

where ν_j is the direction cosine of the normal to the area. The fictitious stresses $\boldsymbol{\sigma}^s_{ij}(\mathbf{x})$ at point $\mathbf{x}$ caused by equivalent forces in domain Ω can be written by using the Green's function as

$$\sigma^s_{ij}(\mathbf{x}) = \int_\Omega \tau^k_{ij}(\mathbf{x}, \mathbf{x}')\bar{F}_k(\mathbf{x}')d\Omega + \int_\Gamma \tau^k_{ij}(\mathbf{x}, \mathbf{x}')\bar{S}_k(\mathbf{x}')d\Gamma$$
$$= -C_{klmn}\int_\Omega \tau^k_{ij}(\mathbf{x}, \mathbf{x}')\epsilon''_{mn,l}(\mathbf{x}')d\Omega$$
$$+ C_{klmn}\int_\Gamma \tau^k_{ij}(\mathbf{x}, \mathbf{x}')\epsilon''_{mn}(\mathbf{x}')\nu_l d\Gamma \tag{3}$$

where $\tau^k_{ij}(\mathbf{x}, \mathbf{x}')$ represents the stress component σ_{ij} at point $\mathbf{x}$ induced by a unit force acting at point $\mathbf{x}'$ along the x_k-axis. Γ is the boundary of domain Ω. If inelastic strain components of $\epsilon''_{mn}(\mathbf{x})$ are constant in Ω, eqn (3) is reduced to

$$\sigma^s_{ij}(\mathbf{x}) = C_{klmn}\left\{\int_\Gamma \tau^k_{ij}(\mathbf{x}, \mathbf{x}')\nu_l d\Gamma\right\}\epsilon''_{mn}(\Omega) \tag{4}$$

where $\epsilon''_{mn}(\Omega)$ is the constant inelastic strain in Ω. The residual stress field is

$$\sigma^r_{ij}(\mathbf{x}) = \sigma^s_{ij}(\mathbf{x}) - C_{ijkl}\epsilon''_{kl}(\mathbf{x}) \tag{5}$$

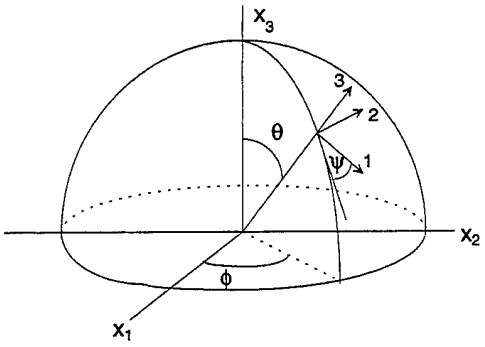

Fig. 3 Euler angles and representation of crystal orientations

3.2 Residual Stress Influence Coefficient. To calculate the residual stress field numerically, the discretization of a continuous problem is needed. In the following, the domain Ω in an extended solid is divided into a number of subdomains or elements Ω_q. In each of them, it is assumed that the inelastic strain ϵ''_{ij} is uniform. After applying Eqs. (4) and (5) to Ω_q, the residual stress field due to $\epsilon''_{mn}(\mathbf{x}')(\mathbf{x}' \in \Omega_q)$ is

$$\sigma^r_{ij}(\mathbf{x}) = \left\{ \int_{\Gamma_q} \mathbf{C}_{klmn} \tau^k_{ij}(\mathbf{x}, \mathbf{x}') \nu_l d\Gamma_q - H(\mathbf{x}, \Omega_q) C_{ijmn} \right\} \epsilon''_{mn}(\Omega_q) \quad (6)$$

where the function $H(\mathbf{x}, \Omega_q)$ is defined as

$$H(\mathbf{x}, \Omega_q) = \begin{cases} 1, & \mathbf{x} \in \Omega_q \\ 0, & \mathbf{x} \notin \Omega_q \end{cases}$$

Generally, residual stress field $\sigma^r_{ij}(\mathbf{x})$ varies from one point to another. The volume average of $\sigma^r_{ij}(\mathbf{x})$ over subdomain Ω_p is taken to represent the residual stresses in element Ω_p. Letting $\sigma^r_{ij}(\Omega_p)$ represent the residual stresses in Ω_p due to ϵ''_{mn} in Ω_q, we have

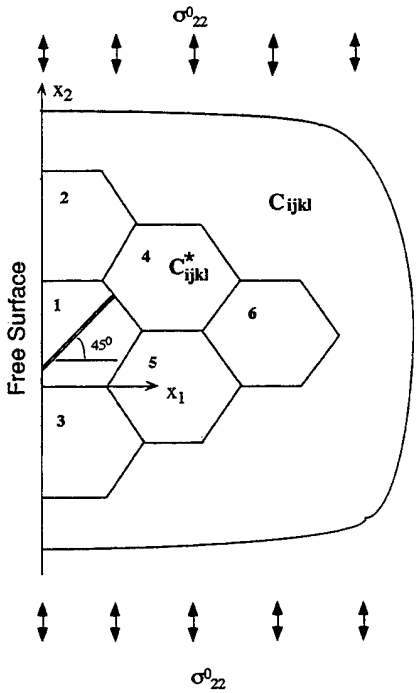

Fig. 4 Polycrystal model of fatigue crack initiation

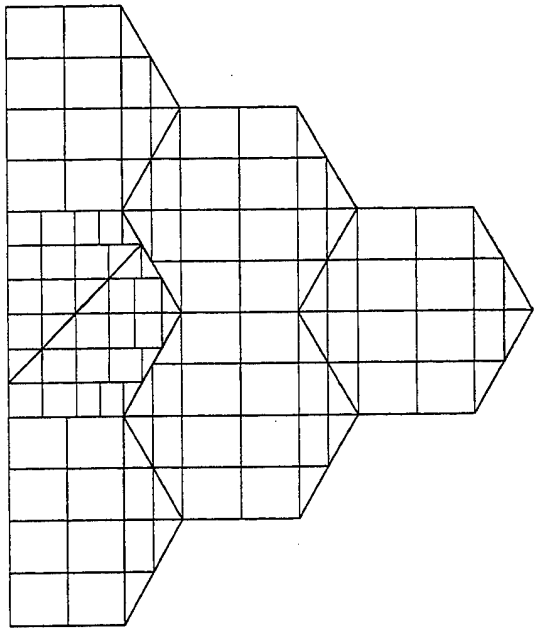

Fig. 5 Layout of elements

$$\sigma^r_{ij}(\Omega_p) = G_{ijmn}(\Omega_p, \Omega_q) \epsilon''_{mn}(\Omega_q) \quad (7)$$

where $G_{ijmn}(\Omega_p, \Omega_q)$ are called the residual stress influence coefficients, which represent the residual stresses in subdomain Ω_p caused by unit inelastic strain components in subdomain Ω_q.

For the resolved residual shear stress $\tau^r_{\alpha\beta}$ in slip system $\alpha\beta$ in Ω_p due to the resolved plastic shear strain $e^p_{\xi\eta}$ in slip system $\xi\eta$ in Ω_q, Eq. (7) can be rewritten by the tensor transformation as

$$\tau^r_{\alpha\beta}(\Omega_p) = G(\alpha\beta, \Omega_p; \xi\eta, \Omega_q) e^p_{\xi\eta}(\Omega_q) \quad (8)$$

where $G(\alpha\beta, \Omega_p; \xi\eta, \Omega_q)$ represents the residual resolved shear stress in slip system $\alpha\beta$ in Ω_p caused by a unit resolved plastic shear strain in slip system $\xi\eta$ in Ω_q. The total resolved shear stress $\tau_{\alpha\beta}$ in slip system $\alpha\beta$ in Ω_p is

$$\tau_{\alpha\beta}(\Omega_p) = \tau^I_{\alpha\beta} + \tau^A_{\alpha\beta} + \sum_q \sum_{\xi\eta} G(\alpha\beta, \Omega_p; \xi\eta, \Omega_q) e^p_{\xi\eta} \quad (9)$$

The summation with regard to slip system $\xi\eta$ includes all the slip systems in Ω_q.

3.3 Generalized Plane Strain Problem. The thickness of fatigue bands is much smaller than the length (dimension along the x_3-axis) as observed at the free surface of metals. Therefore, the problem is considered under the plane strain deformation. The plastic strain due to slip in the secondary slip system is not confined to the x_1x_2 plane. This causes an equivalent force component $\bar{F}_3$ acting along the x_3-direction. The existence of this $\bar{F}_3$ requires a modification of the plane strain problem. Hence, the generalized plane strain problem is considered in the present study. A similar problem is shown in the analysis of prismatic anisotropic bars by Lekhnitski (1963). This generalized plane strain deformation is defined as

$$u_i = u_i(x_1, x_2), \quad i = 1, 2, 3$$

where u_i is the displacement component along x_i-axis. This gives

$$\sigma_{ij} = 2\mu \left\{ \frac{\nu}{1 - 2\nu} \delta_{ij}\theta + \frac{1}{2}(u_{i,j} + u_{j,i}) \right\}$$

where $\theta = u_{1,1} + u_{2,2}$ and ν is the Poisson's ratio. The equilib-

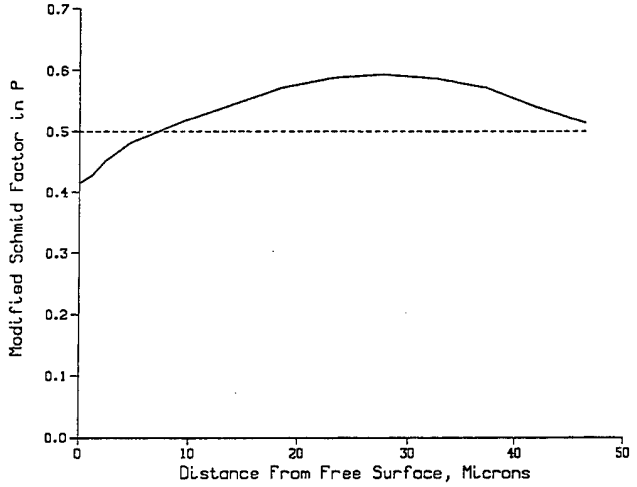

Fig. 6 Modified Schmid factor varying along slice *P*

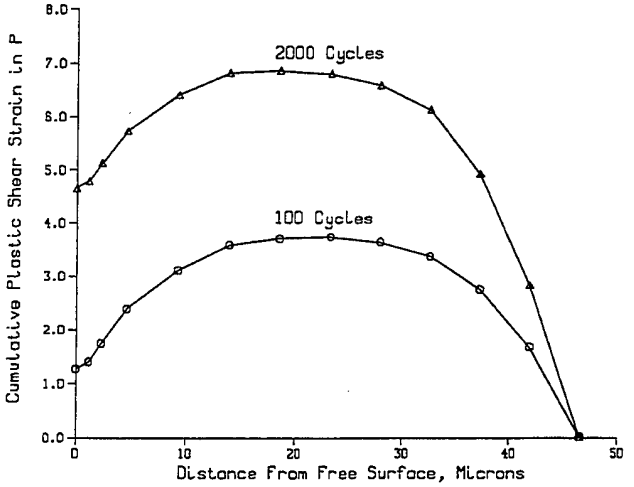

Fig. 8 Plastic shear strain distributions in *P* at 100 cycles and 2000 cycles

rium equations in terms of displacement components u_i can be expressed as

$$\nabla^2 u_i + \frac{1}{1-2\mu}\frac{\partial \theta}{\partial x_i} + \frac{F_i}{\mu} = 0, \quad i = 1, 2 \tag{10}$$

and

$$\nabla^2 u_3 + \frac{F_3}{\mu} = 0 \tag{11}$$

where

$$\nabla^2 = \frac{\partial^2}{\partial x_1^2} + \frac{\partial^2}{\partial x_2^2}$$

and F_i is the body force component. Equations (10) and (11) are not coupled and can be solved separately.

The stress components $\tau_{ij}^k(\mathbf{x}, \mathbf{x}')$ in Eq. (3) for the semi-infinite medium with the generalized plane strain deformation have been expressed in terms of the Airy's stress functions (Lin and Lin, 1974) as

$$\tau_{11}^k(\mathbf{x}, \mathbf{x}') = \frac{\partial^2 \phi_k}{\partial x_2^2}, \quad \tau_{22}^k(\mathbf{x}, \mathbf{x}') = \frac{\partial^2 \phi_k}{\partial x_1^2},$$

$$\tau_{12}^k(\mathbf{x}, \mathbf{x}') = -\frac{\partial^2 \phi_k}{\partial x_1 \partial x_2}, \tau_{33}^k(\mathbf{x}, \mathbf{x}') = \nu \nabla^2 \phi_k,$$

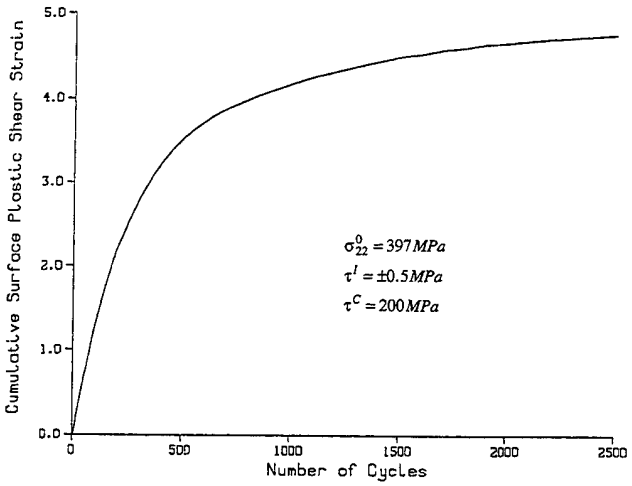

Fig. 7 Plastic shear strain at free surface versus number of cycles

$$\tau_{13}^k(\mathbf{x}, \mathbf{x}') = \tau_{23}^k(\mathbf{x}, \mathbf{x}') \equiv 0, \quad k = 1, 2 \tag{12}$$

and

$$\tau_{13}^3(\mathbf{x}, \mathbf{x}') = \frac{\partial \phi_3}{\partial x_1}, \quad \tau_{23}^3(\mathbf{x}, \mathbf{x}') = \frac{\partial \phi_3}{\partial x_2},$$

$$\tau_{ij}^3(\mathbf{x}, \mathbf{x}') \equiv 0, \quad \text{for other } i \text{ and } j \tag{13}$$

where the Airy's stress functions are

$$\phi_1(\mathbf{x}, \mathbf{x}') = -(p+q)(x_2 - x_2')(\theta_1 + \theta_2) + \tfrac{1}{2}q(x_1 - x_1')\ln(X_1/X_2) + 2px_1x_1'(x_1 + x_1')/X_2$$

$$\phi_2(\mathbf{x}, \mathbf{x}') = (p+q)(x_2 - x_2')(\theta_1 + \theta_2) + \tfrac{1}{2}q(x_2 - x_2')\ln(X_1/X_2) - 2px_1x_1'(x_2 - x_2')/X_2$$

$$\phi_3(\mathbf{x}, \mathbf{x}') = -\frac{1}{4\pi}(\ln X_1 + \ln X_2)$$

with

$$p = \frac{1}{4\pi(1-\nu)}, \quad q = p(1-2\nu)$$

$$\theta_1 = \arctan\left(\frac{x_2 - x_2'}{x_1 - x_1'}\right), \quad -\pi \le \theta_1 < \pi$$

$$\theta_2 = \arctan\left(\frac{x_2 - x_2'}{x_1 + x_1'}\right), \quad -\frac{\pi}{2} \le \theta_2 < \frac{\pi}{2}$$

$$X_1 = (x_1 - x_1')^2 + (x_2 - x_2')^2,$$

$$X_2 = (x_1 + x_1')^2 + (x_2 - x_2')^2$$

By using Eqs. (6), (12) and (13), the residual stresses as well as the residual stress influence coefficients due to the inelastic strains in the element of a specific shape can be readily calculated.

4 Generalization of Equivalent Inclusion Method

Eshelby's equivalent inclusion method (Eshelby, 1957, 1961) is here used to transform an inhomogeneous problem into a homogeneous one by introducing a distribution of eigenstrains (Mura, 1982). Originally, this method was applied to solve the problems with an ellipsoidal inhomogeneity. In the present study, this method is generalized to solve inhomogeneous problems of arbitrary shapes.

In the following, the matrix and vector notation will be used instead of tensor notation for convenience. It is easy to contract a second-order tensor with components G_{ijkl} into a matrix with entries G_{ij} by setting, for instance, $G_{11} = G_{1111}$, $G_{12} = G_{1122}$, $G_{16} = G_{1112} + G_{1121}$ and $G_{61} = G_{1211}$, etc. Vectors are denoted by boldface lowercase Roman or Greek letters and matrices by boldface uppercase Roman letters. The Eshelby's equivalent equation is

$$\mathbf{C}^*(\mathbf{x})[\boldsymbol{\epsilon}^0 + \boldsymbol{\epsilon}(\mathbf{x}) - \boldsymbol{\epsilon}^p(\mathbf{x})] = \mathbf{C}[\boldsymbol{\epsilon}^0 + \boldsymbol{\epsilon}(\mathbf{x}) - \boldsymbol{\epsilon}^*(\mathbf{x}) - \boldsymbol{\epsilon}^p(\mathbf{x})], \mathbf{x} \in \Omega \quad (14)$$

where Ω is an inclusion or a subdomain with the elastic constant $\mathbf{C}^*(\mathbf{x})$ embedded in an extended body D with the isotropic elastic constant $\mathbf{C}$. $\boldsymbol{\epsilon}(\mathbf{x})$ is the disturbance strain, $\boldsymbol{\epsilon}^*(\mathbf{x})$ the eigenstrain, $\boldsymbol{\epsilon}^p(\mathbf{x})$ the plastic strain and $\boldsymbol{\epsilon}^0$ uniform strain from which $\boldsymbol{\sigma}^0 = \mathbf{C}\boldsymbol{\epsilon}^0$ where $\boldsymbol{\sigma}^0$ is the applied far-field stress. The stress $\boldsymbol{\sigma}$ and strain $\boldsymbol{\epsilon}$ are vectors expressed as

$$\boldsymbol{\sigma} = \{\sigma_{11}, \sigma_{22}, \sigma_{33}, \sigma_{23}, \sigma_{13}, \sigma_{12}\}^T$$

$$\boldsymbol{\epsilon} = \{\epsilon_{11}, \epsilon_{22}, \epsilon_{33}, \epsilon_{23}, \epsilon_{13}, \epsilon_{12}\}^T$$

where notation $\{\cdots\}^T$ represents the transposition. Equation (14) shows that the eigenstrain $\boldsymbol{\epsilon}^*(\mathbf{x})$ plays the same role as the plastic strain $\boldsymbol{\epsilon}^p(\mathbf{x})$ does in the homogeneous materials.

When a continuous problem is discretized for the purpose of numerical analysis, the domain of Ω is further divided into N subdomains $\Omega_i (1 \le i \le N)$ called elements, in each of which both the eigenstrain $\boldsymbol{\epsilon}^*$ and plastic strain $\boldsymbol{\epsilon}^p$ are assumed to be uniform. The stresses in element Ω_i caused by the unit eigenstrain $\boldsymbol{\epsilon}^*$ in element Ω_j are the same as those caused by the unit plastic strain $\boldsymbol{\epsilon}^p$. Thus the stress $\boldsymbol{\sigma}_i^r$ in Ω_i induced by both of the eigenstrains and plastic strains in all the elements is

$$\boldsymbol{\sigma}_i^r = \sum_j \mathbf{G}_{ij}\boldsymbol{\epsilon}_j^* + \sum_k \mathbf{G}_{ik}\boldsymbol{\epsilon}_k^p, \quad 1 \le i \le N \quad (15)$$

where

$$\boldsymbol{\epsilon}_j^* = \{\epsilon_{11}^*, \epsilon_{22}^*, \epsilon_{33}^*, \epsilon_{23}^*, \epsilon_{13}^*, \epsilon_{12}^*\}_j^T$$

$$\boldsymbol{\epsilon}_j^p = \{\epsilon_{11}^p, \epsilon_{22}^p, \epsilon_{33}^p, \epsilon_{23}^p, \epsilon_{13}^p, \epsilon_{12}^p\}_j^T$$

in Ω_j and $\mathbf{G}_{ij}$ are 6×6 matrices of the residual stress influence coefficients, which are contracted from $G_{klmn}(\Omega_i, \Omega_j)$.

For the generalized plane strain problem, u_3 does not vary along the x_3-direction. The total normal strain component ϵ_{33}^T is equal to zero. The strain component ϵ_{33}^0 is here taken to be zero.

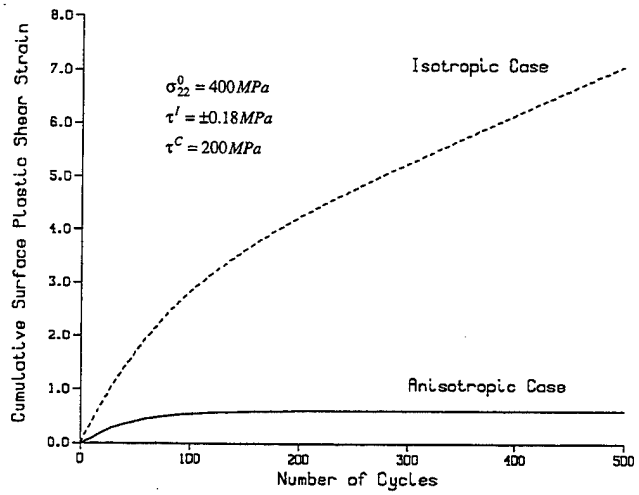

Fig. 9 Comparison of surface plastic strains with and without considering crystal anisotropy

Since the total strain ϵ_{33}^T is the sum of ϵ_{33}^0 and ϵ_{33}, hence $\epsilon_{33} \equiv 0$. The stress-strain relation may be given as

$$\boldsymbol{\sigma}_i^r = \bar{\mathbf{C}}\boldsymbol{\epsilon}_i - \mathbf{C}(\boldsymbol{\epsilon}_i^* + \boldsymbol{\epsilon}_i^p) \quad (16)$$

where

$$\bar{\mathbf{C}} = \begin{bmatrix} \lambda+2\mu & \lambda & 0 & 0 & 0 \\ \lambda & \lambda+2\mu & 0 & 0 & 0 \\ \lambda & \lambda & 0 & 0 & 0 \\ 0 & 0 & 2\mu & 0 & 0 \\ 0 & 0 & 0 & 2\mu & 0 \\ 0 & 0 & 0 & 0 & 2\mu \end{bmatrix},$$

$$\mathbf{C} = \begin{bmatrix} \lambda+2\mu & \lambda & \lambda & 0 & 0 & 0 \\ \lambda & \lambda+2\mu & \lambda & 0 & 0 & 0 \\ \lambda & \lambda & \lambda+2\mu & 0 & 0 & 0 \\ 0 & 0 & 0 & 2\mu & 0 & 0 \\ 0 & 0 & 0 & 0 & 2\mu & 0 \\ 0 & 0 & 0 & 0 & 0 & 2\mu \end{bmatrix}$$

and

$$\boldsymbol{\epsilon}_i = \{\epsilon_{11}, \epsilon_{22}, \epsilon_{23}, \epsilon_{13}, \epsilon_{12}\}_i^T \quad \text{with} \quad \epsilon_{33} \equiv 0$$

From Eqs. (15) and (16), expressing the disturbance strains $\boldsymbol{\epsilon}_i$ in Ω_i in terms of $\boldsymbol{\epsilon}_j^*$ and $\boldsymbol{\epsilon}_k^p$, we obtain

$$\boldsymbol{\epsilon}_i = \bar{\mathbf{C}}^{-1}[\mathbf{C}(\boldsymbol{\epsilon}_i^* + \boldsymbol{\epsilon}_i^p) + \sum_j \mathbf{G}_{ij}\boldsymbol{\epsilon}_j^* + \sum_k \mathbf{G}_{ik}\boldsymbol{\epsilon}_k^p], \quad 1 \le i \le N \quad (17)$$

where

$$\bar{\mathbf{C}}^{-1} = \frac{1}{\mathrm{E}} \begin{bmatrix} 1 & -\nu & -\nu & 0 & 0 & 0 \\ -\nu & 1 & -\nu & 0 & 0 & 0 \\ 0 & 0 & 0 & 1+\nu & 0 & 0 \\ 0 & 0 & 0 & 0 & 1+\nu & 0 \\ 0 & 0 & 0 & 0 & 0 & 1+\nu \end{bmatrix}$$

in which E is the Young's modulus.

The left-hand side of Eq. (14) can also be written for the generalized plane strain problems as

$$\boldsymbol{\sigma}_i = \boldsymbol{\sigma}_i^* + \bar{\mathbf{C}}^*\boldsymbol{\epsilon}_i - \mathbf{C}^*\boldsymbol{\epsilon}_i^p \quad (18)$$

where $\mathbf{C}^*$ is a 6×6 anisotropic elastic stiffness matrix and $\bar{\mathbf{C}}^*$ a 6×5 matrix formed from matrix $\mathbf{C}^*$ by taking the third column away. And $\boldsymbol{\sigma}_i^* = \bar{\mathbf{C}}^*\boldsymbol{\epsilon}^0$ in which

$$\epsilon^0 = \{\epsilon_{11}^0, \epsilon_{22}^0, \epsilon_{23}^0, \epsilon_{13}^0, \epsilon_{12}^0\}^T \quad \text{with} \quad \epsilon_{33}^0 \equiv 0$$

Substituting Eq. (17) into Eq. (18) and Eq. (15), Eq. (14) becomes

$$\mathbf{T}\boldsymbol{\epsilon}_i^* + \sum_j \mathbf{S}_{ij}\boldsymbol{\epsilon}_j^* = \mathbf{q}_i + (\mathbf{C}^* - \mathbf{T})\boldsymbol{\epsilon}_i^p - \sum_k \mathbf{S}_{ik}\boldsymbol{\epsilon}_k^p, \quad 1 \le i \le N \quad (19)$$

where

$$\mathbf{T} = \bar{\mathbf{C}}^*\bar{\mathbf{C}}^{-1}\mathbf{C}$$

$$\mathbf{S}_{ij} = (\bar{\mathbf{C}}^*\bar{\mathbf{C}}^{-1} - \mathbf{I})\mathbf{G}_{ij}$$

$$\mathbf{q}_i = \boldsymbol{\sigma}^0 - \boldsymbol{\sigma}_i^*$$

$$\boldsymbol{\sigma}^0 = \bar{\mathbf{C}}\boldsymbol{\epsilon}^0$$

and $\mathbf{I}$ is a 6×6 unit matrix.

It can be seen that eigenstrains $\boldsymbol{\epsilon}_i^*$ depend on the applied load $\boldsymbol{\sigma}^0$ and the distribution of plastic strains $\boldsymbol{\epsilon}_k^p$ as well. Equation (19) is a set of linear algebraic equations with unknowns

ϵ_i^*. Solving these equations for ϵ_i^* in all elements Ω_i, we can express ϵ_i^* as

$$\epsilon_i^* = \mathbf{p}_i + \sum_k \mathbf{R}_{ik}\epsilon_k^p, \quad 1 \le i \le N \tag{20}$$

where $\mathbf{p}_i$ is a vector in terms of σ^0 in Ω_i and $\mathbf{R}_{ik}$ is the matrix relating the plastic strains ϵ_k^p in Ω_k to the eigenstrains ϵ_i^* in Ω_i. The total stress in Ω_i, obtained by substituting Eq. (20) into Eq. (15), is

$$\begin{aligned}\sigma_i &= \sigma^0 + \sigma_i^r \\ &= \sigma^0 + \sum_j \mathbf{G}_{ij}\mathbf{p}_j + \sum_k \left(\mathbf{G}_{ik} + \sum_j \mathbf{G}_{ij}\mathbf{R}_{jk}\right)\epsilon_k^p\end{aligned} \tag{21}$$

In the above equation, the term of $\Sigma\, \mathbf{G}_{ij}\mathbf{p}_j$ is a modification to the effect of the applied load σ^0 and $\Sigma\, \mathbf{G}_{ij}\mathbf{R}_{jk}$ the one to the matrix $\mathbf{G}_{ik}$ of the residual stress influence coefficients due to the inhomogeneity.

Under the stress component σ_{22}^0 alone, Eq. (21) reduces to

$$\sigma_i = \bar{\mathbf{p}}_i\sigma_{22}^0 + \sum_k \bar{\mathbf{G}}_{ik}\epsilon_k^p$$

where

$$\bar{\mathbf{p}}_i\sigma_{22}^0 = \sigma^0 + \sum_j \mathbf{G}_{ij}\mathbf{p}_j$$

and

$$\bar{\mathbf{G}}_{ik} = \mathbf{G}_{ik} + \sum_j \mathbf{G}_{ij}\mathbf{R}_{jk}$$

For slip system $\alpha\beta$ in element Ω_i, we have

$$\epsilon_i^p = \mathbf{m}_{\alpha\beta}e_{\alpha\beta i}^p$$

forming the inhomogeneous problem into a homogeneous one. The summation with regard to slip system $\xi\eta$ includes all the slip systems in kth element. It can be seen that Eq. (22) corresponds to Eq. (9).

5 Effect of Crystal Elastic Anisotropy on Fatigue Crack Initiation in Polycrystals

5.1 Elastic Constants of Monocrystalline and Polycrystalline Crystals. In the present study, nickel-base superalloy polycrystals of FCC structure are taken for the numerical analysis. Fatigue crack initiation of other materials can be analyzed by the same approach.

There are many experimental data available for nickel-base superalloy single crystals in the literature. Since the alloy compositions vary with different materials tested, the elastic constants obtained may slightly differ from each other. In the following analysis, the elastic constants of a nickel-base superalloy Ni_3Al single crystal given by Yang (1985) are used. The elastic compliance moduli in $10^{-2}/GPa$ with respect to the crystal axes [001], [010] and [100] in the same notation as Yang's are

$$S_{11} = S_{1111} = 1.01$$

$$S_{12} = S_{1122} = -0.393$$

$$S_{44} = 4S_{1212} = 0.848$$

The crystal orientations with respect to the loading axes (fixed coordinates) are represented by the Euler angles (θ, ϕ, ψ) as shown in Fig. 3. The global elastic compliance in tensor notation is

$$\mathbf{L} = [l_{i\alpha}] = \begin{bmatrix} \cos\theta\cos\phi\cos\psi - \sin\phi\sin\psi, & -\cos\theta\cos\phi\sin\psi - \sin\phi\cos\psi, & \sin\theta\cos\phi \\ \cos\theta\sin\phi\cos\psi + \cos\phi\sin\psi, & -\cos\theta\sin\phi\sin\psi + \cos\phi\cos\psi, & \sin\theta\sin\phi \\ -\sin\theta\cos\psi, & \sin\theta\sin\psi & \cos\theta \end{bmatrix}$$

and

$$\tau_{\alpha\beta i} = \mathbf{n}_{\alpha\beta}^T\sigma_j$$

where $e_{\alpha\beta i}^p$ and $\tau_{\alpha\beta i}$ are the plastic shear strain and resolved shear stress, respectively, and

$$\mathbf{m}_{\alpha\beta} = \{m_{11}, m_{22}, m_{33}, m_{23}, m_{13}, m_{12}\}_{\alpha\beta}^T$$

$$\mathbf{n}_{\alpha\beta} = \{n_{11}, n_{22}, n_{33}, n_{23}, n_{13}, n_{12}\}_{\alpha\beta}^T$$

in which m_{ij} and n_{ij} are composed of direction cosines of slip system $\alpha\beta$. The total resolved shear stress in the slip system is

$$\tau_{\alpha\beta i} = \tau_{\alpha\beta i}^I + \tau_{\alpha\beta i}^A + \tau_{\alpha\beta i}^R \tag{22}$$

in which

$$\tau_{\alpha\beta i}^A = \mathbf{n}_{\alpha\beta}^T\bar{\mathbf{p}}_i\sigma_{22}^0 = s_{\alpha\beta i}\sigma_{22}^0$$

$$\tau_{\alpha\beta i}^R = \sum_k \sum_{\xi\eta} \bar{G}(\alpha\beta, \Omega_j; \xi\eta, \Omega_k)e_{\xi\eta k}^p$$

where $s_{\alpha\beta i}$ is the modified Schmid factor with the consideration of anisotropic elastic constants and $\bar{G}(\alpha\beta, \Omega_i; \xi\eta, \Omega_j)$ expressed as

$$\bar{G}(\alpha\beta, \Omega_i; \xi\eta, \Omega_k) = \mathbf{n}_{\alpha\beta}^T\bar{\mathbf{G}}_{ik}\mathbf{m}_{\xi\eta}$$

are the modified residual stress influence coefficients after trans-

$$\bar{S}_{ijkm} = l_{i\alpha}l_{j\beta}l_{k\lambda}l_{m\gamma}S_{\alpha\beta\lambda\gamma} \tag{23}$$

where

The inverse of $\bar{S}_{ijkm}$ is the elastic stiffness modulus. Equation (23) was used to obtain the elastic stiffness matrices of single crystals referring to the specimen axes.

A range of test data of the Young's modulus and shear modulus of Ni_3Al polycrystal and its alloys are found in the article by Stoloff (1989). The isotropic elastic constants of Poisson's ratio, $\nu = 0.3$, and shear modulus, $\mu = 65$ GPa, are here used for our analysis of Ni_3Al polycrystals.

5.2 Physical Model and Numerical Results. A physical model to study the elastic anisotropy and inhomogeneity of crystals on the fatigue crack initiation in a polycrystal is shown in Fig. 4. An aggregate of crystals with various crystallographic orientations is embedded near the free surface in a semi-infinite elastic medium. The cross-sections of these crystals are either whole or part of a hexagon. Since the crystals at some distance away from the surface crystal, in which a fatigue band is analyzed, are randomly oriented, these surrounding crystals are assumed to be isotropic and homogeneous. The fatigue band is composed of three thin slices P, Q, and R. The orientation of surface crystal #1 is determined by the orientation of the primary slip system, which is 45 deg inclining to x_2-axis. The elastic stiffness matrix of this crystal with respect to the loading axes is

$$\mathbf{C}^* = \begin{bmatrix} 244.33 & 118.19 & 83.91 & -27.42 & -82.29 & -13.71 \\ 118.19 & 244.33 & 83.91 & 82.29 & 27.43 & -13.71 \\ 83.91 & 83.91 & 278.61 & -54.86 & 54.86 & 27.43 \\ -13.71 & 41.14 & -27.43 & 153.56 & 27.43 & 27.43 \\ -41.14 & 13.71 & 27.43 & 27.43 & 153.56 & -27.43 \\ -6.86 & -6.86 & 13.71 & 27.43 & -27.43 & 222.13 \end{bmatrix} \; GPa$$

The surface crystal with the fatigue band and the surrounding crystals are shown in Fig. 4. The fatigue band is divided into parallelogram elements and the remaining parts of the crystals are divided into trapezoidal elements. The paralellogram elements are assumed to have linear inelastic strains and the trapezoidal elements to have constant inelastic strains. Fig. 5 shows the layout of these elements in the aggregate.

The local stresses in the surface crystal containing the fatigue band are affected not only by the applied load but also by the orientations of its surrounding grains. Plastic strains can develop both inside and outside the fatigue band and the residual stresses are affected by the orientations of the surrounding crystals. The global elastic stiffness matrix of crystals of the orientation (θ, ϕ, ψ) is denoted as $\mathbf{C}^*(\theta, \phi, \psi)$.

The surrounding crystals can have different sets of orientations. In the following, one set is calculated to illustrate the effect of anisotropy and inhomogeneity on the fatigue crack initiation. In this set, the orientation of crystals #2 and #3 is chosen to be (60, 30, 30 deg), crystals #4 and #5 to be (0, 0, 0 deg) and crystal #6 to be (30, 30, 60 deg). The global elastic stiffness matrices of crystals with these orientations are listed as follows

$$\mathbf{C}^*(60, 30, 30 \text{ deg}) = \begin{bmatrix} 279.50 & 79.49 & 87.44 & -75.16 & -29.89 & -4.18 \\ 79.49 & 300.71 & 66.23 & 19.49 & 26.04 & 20.88 \\ 87.44 & 66.23 & 292.76 & 55.67 & 3.86 & -16.70 \\ -37.58 & 9.74 & 27.84 & 118.20 & -16.70 & 26.04 \\ -14.95 & 13.02 & 1.93 & -16.70 & 160.63 & -75.16 \\ -2.09 & 10.44 & -8.35 & 26.04 & -75.16 & 144.72 \end{bmatrix} \; GPa$$

$$\mathbf{C}^*(0, 0, 0 \text{ deg}) = \begin{bmatrix} 196.33 & 125.05 & 125.05 & 0.0 & 0.0 & 0.0 \\ 125.05 & 196.33 & 125.05 & 0.0 & 0.0 & 0.0 \\ 125.05 & 125.05 & 196.33 & 0.0 & 0.0 & 0.0 \\ 0.0 & 0.0 & 0.0 & 235.85 & 0.0 & 0.0 \\ 0.0 & 0.0 & 0.0 & 0.0 & 235.85 & 0.0 \\ 0.0 & 0.0 & 0.0 & 0.0 & 0.0 & 235.85 \end{bmatrix} \; GPa$$

$$\mathbf{C}^*(30, 30, 60 \text{ deg}) = \begin{bmatrix} 247.36 & 122.16 & 76.91 & -19.78 & 80.57 & 7.28 \\ 122.16 & 216.65 & 107.62 & 69.81 & -11.74 & 15.07 \\ 76.91 & 107.62 & 261.90 & -50.03 & -68.83 & -22.35 \\ -9.89 & 34.91 & -25.01 & 201.00 & -22.35 & -11.74 \\ 40.29 & -5.87 & -34.42 & -22.35 & 139.56 & -19.78 \\ 3.64 & 7.54 & -11.17 & -11.74 & -19.78 & 230.06 \end{bmatrix} \; GPa$$

With the method described, the modified Schmid factor $s_{\alpha\beta}$ of the primary slip system varying along slice P is shown in Fig. 6. The Schmid factor varies from 0.42 at the free surface to the maximum value of 0.59. It is seen that the effect of this anisotropy on the response to the applied load makes the Schmid factor greater than 0.5 in a large part of the slice. The drop of the modified Schmid factor close to the free surface seems to be due to the less constraint on the deformation near the surface than in the interior. Without considering the crystal anisotropy, the Schmid factor is uniformly 0.5. The increase of the Schmid factor decreases the applied load required to activate the plastic slip in the band in comparison with the isotropic and homogeneous case. The region in which the total resolved shear stress reaches the critical shear stress τ^C will slide first. Therefore, the sliding starts inside the band, where the Schmid factor takes the maximum value. The case, in which $\sigma_{22}^0 = 397MPa$, $\tau^I = \pm 0.5MPa$ and $\tau^C = 200MPa$, was analyzed. The surface plastic resolved shear strain vs. the number of cycles is shown in Fig. 7. If crystal anisotropy is neglected, the fatigue band will not develop in the surface crystal under the applied load. Therefore, the threshold of fatigue crack initiation is lowered with the consideration of crystal anisotropy. Fig. 8 shows the plastic resolved shear strain distributions in P at 100 cycles and 2000 cycles, respectively.

The cumulative surface plastic shear strains versus the number of loading cycles for two cases, one with the consideration of crystal anisotropy and one without, were calculated and plotted in Fig. 9. It is seen that the neglect of the crystal anisotropy in a polycrystal may cause significant error in calculating the slip distribution and in estimating the fatigue crack initiation.

Acknowledgment

This research is supported by the U. S. Air Force Office of Scientific Research Grant F49620-92-0171. The interest of Dr. Jim Chang, Dr. Walter Jones and Dr. Spencer Wu is gratefully acknowledged.

References

Antonopoulos, J. G., Brown, L. M., and Winter, A. T., 1976, "Vacancy Dipoles in Fatigued Copper," *Philosophical Magazine*, Vol. A34, pp. 549–563.

Charsley, P., and Thompson, N., 1963, "The Behavior of Slip Lines on Aluminum Crystals under Reversed Stresses in Tension and Compression," *Philosophical Magazine*, Vol. 8, pp. 77–85.

Eshelby, J. D., 1957, "The Determination of the Elastic Field of an Ellipsoid, and related Problems," *Proc. Roy. Soc.*, Vol. A241, pp. 376–396.

Eshelby, J. D., 1961, "Elastic Inclusions and Inhomogeneities," *Progress in Solid Mechanics 2*, I. N. Snedden and R. Hill, eds., North-Holland, Amsterdam, pp. 89–140.

Forsyth, P. J. E., 1954, "Some Further Observations on the Fatigue Process in Pure Aluminum," *J. Inst. Met.*, Vol. 82, pp. 449–454.

Lekhnitski, S. G., 1963, *Theory of Elasticity of an Anisotropic Body,* Holden-Day, San Francisco, pp. 129–134.

Lin, S. R., and Lin, T. H., 1983, "Initial Strain Field and Fatigue Crack Initiation Mechanics," ASME *Journal of Applied Mechanics,* Vol. 50, pp. 367–372.

Lin, T. H., 1969, *Theory of Inelastic Structures,* Wiley, New York, pp. 44–48.

Lin, T. H., 1977, "Micromechanics of Deformation of Slip Bands under Monotonic and Cyclic Loading," *Reviews of the Deformation Behavior of Materials,* P. Felham, ed., Freund Publishing House, Tel-Aviv, Israel, pp. 263–316.

Lin, T. H., 1992, "Micromechanics of Crack Initiation in High-Cycle Fatigue," *Advances in Applied Mechanics,* Vol. 29, pp. 1–62.

Lin, T. H., and Ito, Y. M., 1969, "Mechanics of Fatigue Crack Nucleation Mechanism," *J. Mech. Phys. Solids,* Vol. 17, pp. 511–523.

Lin, T. H., and Lin, S. R., 1974, "Effect of Secondary Slip Systems on Early Fatigue Damage," *J. Mech. and Phys. Solids,* Vol. 22, pp. 177–192.

Lin, T. H., Lin, S. R., and Wu, X. Q., 1989, "Micromechanics of an Extrusion in High-Cycle Fatigue," *Philosophical Magazine,* Vol. A59, pp. 1263–1276.

Mughrabi, H., Wang, R., Differt, K., and Essmann, V., 1982, "Fatigue Crack Initiation by Cyclic Slip Irreversibilities in High-Cycle Fatigue," *Fatigue Mechanisms: Advances in Quantitative Measurement of Physical Damage,* ASTM STP 811, J. Lankford, D. J. Davidson, W. L. Morris, and R. P. Wei, eds., pp. 5–45.

Mura, T., 1982, *Micromechanics of Defects in Solids,* Martinus Nijhoff Publishers. pp. 150–159.

Parker, E. R., 1961, *Mechanical Behavior of Materials at Elevated Temperatures,* J. E. Dorn, ed., McGraw-Hill, New York, pp. 129–148.

Stoloff, N. S., 1989, "Physical and Mechanical Metallurgy of Ni_3Al and its Alloys," *Int. Mater. Res.,* Vol. 34, pp. 153–183.

Yang, S. W., 1985, "Elastic Constants of a Monocrystalline Nickel-Base Superalloy," *Metallurgical Transactions A,* Vol. 16A, pp. 661–665.